Thin-film thermoelectric devices with high room-temperature figures of merit

Rama Venkatasubramanian, Edward Siivola, Thomas Colpitts & Brooks O'Quinn

Research Triangle Institute, Research Triangle Park, North Carolina 27709, USA

Thermoelectric materials are of interest for applications as heat pumps and power generators. The performance of thermoelectric devices is quantified by a figure of merit, *ZT*, where *Z* is a measure of a material's thermoelectric properties and *T* is the absolute temperature. A material with a figure of merit of around unity was first reported over four decades ago, but since then—despite investigation of various approaches—there has been only modest progress in finding materials with enhanced *ZT* values at room temperature. Here we report thin-film thermoelectric materials that demonstrate a significant enhancement in *ZT* at 300 K, compared to state-of-the-art bulk Bi_2Te_3 alloys. This amounts to a maximum observed factor of ~2.4 for our p-type Bi_2Te_3/Sb_2Te_3 superlattice devices. The enhancement is achieved by controlling the transport of phonons and electrons in the superlattices. Preliminary devices exhibit significant cooling (32 K at around room temperature) and the potential to pump a heat flux of up to 700 W cm^{-2}; the localized cooling and heating occurs some 23,000 times faster than in bulk devices. We anticipate that the combination of performance, power density and speed achieved in these materials will lead to diverse technological applications: for example, in thermochemistry-on-a-chip, DNA microarrays, fibre-optic switches and microelectrothermal systems.

The performance of thermoelectric devices depends on the figure of merit (ZT) of the material, given by

$$ZT = (\alpha^2 T/\rho K_T) \quad (1)$$

where α, T, ρ and K_T are the Seebeck coefficient, absolute temperature, electrical resistivity and total thermal conductivity, respectively. Z, the material coefficient, can be expressed in terms of lattice thermal conductivity (K_L), electronic thermal conductivity (K_e) and carrier mobility (μ), for a given carrier density (p) and the corresponding α, yielding equation (2), below. Here L_0 is the Lorenz number, approximately 1.5×10^{-8} V^2 K^{-2} in non-degenerate semiconductors, q is the electronic charge, and σ is electrical conductivity.

$$Z = \frac{\alpha^2\sigma}{K_L + K_e} \simeq \frac{\alpha^2}{\left(\frac{K_L}{\mu p q}\right) + L_0 T} \quad (2)$$

State-of-the-art devices utilize alloys, typically p-$Bi_xSb_{2-x}Te_{3-y}Se_y$ ($x\approx0.5$, $y\approx0.12$) and n-$Bi_2(Se_yTe_{1-y})_3$ ($y\approx0.05$) for the 200–400 K temperature range. For certain alloys, K_L can be reduced more strongly than μ, leading[1] to enhanced ZT. A ZT of 0.75 at 300 K in p-type $Bi_xSb_{2-x}Te_3$ ($x\approx1$) was reported[2] 40 years ago. Since then, there has been modest progress in the ZT of thermoelectric materials near 300 K. The highest ZT in any bulk thermoelectric material at 300 K appears to be ~1.14 for p-type $(Bi_2Te_3)_{0.25}(Sb_2Te_3)_{0.72}(Sb_2Se_3)_{0.03}$ alloy[3], although there has been a report[4] of an estimated $ZT>2$ at 300 K in $Bi_{0.5}Sb_{1.5}Te_3$ alloy under a hydrostatic pressure of 2 GPa. A ZT value of greater than one in crystals of Bi–Sb alloy under a magnetic field[5] at ~100 K has been reported. There is no apparent thermodynamic upper limit on ZT; in addition to its engineering importance, values of ZT significantly larger than unity are of interest to transport theory[6].

Several possible approaches to enhancing ZT have been investigated. In bulk materials, cage-like structures simulating a phonon glass/electron crystal[7] have been examined, with a view to reducing K_L without a deterioration of the electronic mobilities. A value of $ZT>1$ in $LaFe_3CoSb_{12}$ was reported[8] at $T>700$ K, and attributed primarily to reduction of K_L from La-filling[9]. A ZT of ~1.35 was reported for the skuterrudite $CeFe_{3.5}Co_{0.5}Sb_{12}$ at ~900 K (ref. 10) where, although a dramatic reduction in K_L of the filled skuterrudite was observed near 300 K, there was apparently less role of Ce-filling at higher temperatures where the enhanced ZT was observed. A ZT of ~0.8 at 225 K was observed[11] in $CsBi_4Te_6$, significantly higher than in $Bi_{0.5}Sb_{1.5}Te_3$, apparently due to the smaller bandgap of the former compound (M.G. Kanatzidis, personal communication). From these results, we observe the following: (1) A ZT significantly greater than 1 has not been demonstrated at ordinary temperatures (300 K). (2) A one-to-one correlation between lower K_L and enhanced ZT has not been established. (3) More importantly, the concept of individually tailoring the phonon properties without producing a deterioration of electronic transport, thereby enhancing ZT, has not been established.

Thin-film thermoelectric materials[12] offer tremendous scope for ZT enhancement. Three generic approaches have been proposed to date. One involves the use of quantum-confinement effects[13] to obtain an enhanced density of states near the Fermi energy. Using such effects, a ZT of 0.9 at 300 K and 2.0 at 550 K, using estimated thermal-conductivity values, has been reported[14] in $PbSe_{0.98}Te_{0.02}$/PbTe quantum-dot structures. The second approach[15] involves phonon-blocking/electron-transmitting superlattices. These structures utilize the acoustic mismatch between the superlattice components to reduce K_L (refs 16, 17), rather than using the conventional alloying approach, thereby potentially eliminating alloy scattering of carriers. The third thin-film approach is based on thermionic effects in heterostructures[18,19]. Here we report a ZT at 300 K of ~2.4 in p-type Bi_2Te_3/Sb_2Te_3 superlattices and a similar, although less dramatic, $ZT\approx1.4$ in n-type $Bi_2Te_3/Bi_2Te_{2.83}Se_{0.17}$ superlattices. These ZT values were measured in devices using the Harman technique[20], in which parameters related to ρ, K_T and α (that make up ZT) are measured at the same place, at the same time, with current flowing. This method has been extended with a variable-thickness approach (C.B. Vining, personal communication) to obtain the intrinsic ZT and other parameters.

Potential ideality of superlattices in the Bi_2Te_3 system

High-quality superlattices have been produced[21,22] in the Bi_2Te_3 system, with one of the individual layers as small as 10 Å, using a low-temperature growth process. Such ultra-short-period superlattices offer significantly higher in-plane carrier mobilities (parallel to the superlattice interfaces) than alloys, owing to the near absence of alloy scattering and random interface carrier scattering[23]. We show that the enhanced carrier mobilities in monolayer-range superlattices are effective in the cross-plane direction for certain

© 2001 Macmillan Magazines Ltd

superlattices, where we can also obtain reduced K_L and so an enhanced ZT as per equation (2).

We adapted the transmission line model (TLM) technique[23] used for the measurement of specific electrical contact resistivities (ρ_c)[24] to determine the cross-plane electrical transport. This adaptation was feasible with the low ρ_c ($< 10^{-7}\,\Omega\,cm^2$) achievable in these materials. With such ρ_c, the transfer lengths (L_t) are small, and so an effective 'squeezing' of the current occurs. A typical TLM device consists of adjacent metallized areas, spaced a few micrometres apart, serving as top current-injection contacts. The current is confined to the thin-film on the substrate. The film between the contacts is etched anisotropically to create various device thickness underneath the contacts[23]. Measuring the intercept resistances using successive etch-steps gives the electrical resistivity perpendicular to the superlattice interfaces. We observe that the average length of the contact is ~250 μm, much greater than L_t (~1 μm). Thus the top metal contact, the thermally conducting substrate, and the inactive (where current is not flowing) thermoelectric material act like thermal shunts, in addition to exacerbated radiative/convective losses from the close-to-surface L_t region, for any cooling developed across this region. Thus we have performed an isothermal electrical resistivity measurement, confirmed by negligible Peltier voltage (in a Harman method[20] set-up) in such TLM structures. Further, the cross-plane electrical resistivities determined by the TLM method were confirmed by the variable-thickness ZT method in some of the high-ZT samples, as discussed subsequently. This method has been tested on n-Bi_2Te_3 thin films with known theoretical and experimental electrical anisotropy[25]; we measured an anisotropy of 3.8 ± 0.32 and the theoretical anisotropy is ~4.1 (ref. 25). The validity was also confirmed in p-type $Bi_xSb_{2-x}Te_3$ ($x \approx 0.63 \pm 0.12$) alloy[26] films.

The anticipated heterostructure band diagram in these short-period/shallow potential superlattices is shown in Fig. 1a, where the valence-band offset is expected to be less than the average thermal energy of carriers. The variation of the mobility anisotropy as a function of superlattice period, for $d_{Bi_2Te_3} = d_{Sb_2Te_3}$, is shown in Fig. 1b. $d_{Bi_2Te_3}$ and $d_{Sb_2Te_3}$ are the thickness of the Bi_2Te_3 and Sb_2Te_3 layers, respectively, that make up a period. The carrier concentration is isotropic, so the ratio of electrical resistivity anisotropy is inversely related to the mobility anisotropy (or $\mu_\perp/\mu_{in\text{-}plane}$, where $\mu_\perp$ is the cross-plane mobility). The mobility anisotropies of the 10Å/10Å, 10Å/20Å, 10Å/50Å, 20Å/20Å, 20Å/30Å and 20Å/40Å structures are shown in Fig. 1c. (Here 10 Å/50 Å, for example, indicates $d_{Bi_2Te_3} = 10$ Å and $d_{Sb_2Te_3} = 50$ Å in the superlattice.) The measured cross-plane mobilities in the Bi_2Te_3/Sb_2Te_3 superlattices appear to be consistent with a miniband conduction across the superlattice interfaces, with fully developed or larger valence-band offsets in structures for Bi_2Te_3 thickness ≥30 Å. The data are qualitatively similar to the transport models developed for AlGaAs/GaAs superlattices[27,28]. Note from Fig. 1b, c that the 10Å/50Å, 20Å/40Å and 10Å/20Å Bi_2Te_3/Sb_2Te_3 superlattices offer cross-plane electrical conductivities comparable to in-plane values. It has been shown[29] that periods of 50–60 Å are desirable for minimizing K_L; thus the 10Å/50Å and 20Å/40Å superlattices are useful for enhanced ZT.

Bi_2Te_3/Sb_2Te_3 superlattices show significantly reduced K_L. A full description of the measurement procedure, the data, and the mechanisms are presented elsewhere[29]. The behaviour of these superlattices are consistent with phonon-transmission experiments in GaAs/AlGaAs superlattices[30], although we have invoked coherent backscattering of phonons at superlattice interfaces[29], similar to photon-localization in highly scattering media[31,32]. Values of K_L of the superlattice structures show a minimum of ~0.22 $W\,m^{-1}\,K^{-1}$ at ~50 Å; this is a factor of 2.2 smaller than the K_L of $Bi_{0.5}Sb_{1.5}Te_3$ alloy (~0.49 $W\,m^{-1}\,K^{-1}$) along the same c axis. We note that a theory for the thermal conductivity minimum has been proposed[33]. K_L for all the 60-Å-period structures, whether it be 30Å/30Å or 10Å/50Å or 20Å/40Å, is about 0.25 $W\,m^{-1}\,K^{-1}$. K_L appears to be more dependent on the superlattice period[29], relatively independent of the thickness of the constituents, whereas the electronic transport depends on the period and the relative thickness of the constituents (Fig. 1b, c).

A K_L value of 0.22 $W\,m^{-1}\,K^{-1}$ can be compared with the minimum thermal conductivities (K_{min}) predicted for Bi_2Te_3, using the full-wavelength or half-wavelength models of Slack[34] and Cahill[35] for the phonon mean free path. Table 1 shows these predicted values, along with experimental K_L values of alloys along the trigonal axis (c axis) or perpendicular to it (a-b axis). The K_L values in the superlattices approach the values of K_{min} estimated from the models of Slack and Cahill. When all the phonons have a mean free path equal to the lattice spacing, K_{min} is expected[36] to be between the predictions of the models of Slack and Cahill. The phonon mean free path from kinetic theory is approximately 2.2 Å, using a K_L of 0.22 $W\,m^{-1}\,K^{-1}$ (ref. 29), assuming that all phonons have similar mean free paths—this is justifiable, given that the Debye temperature of Bi_2Te_3 is ~160 K, far lower than the temperature of measurement (300 K).

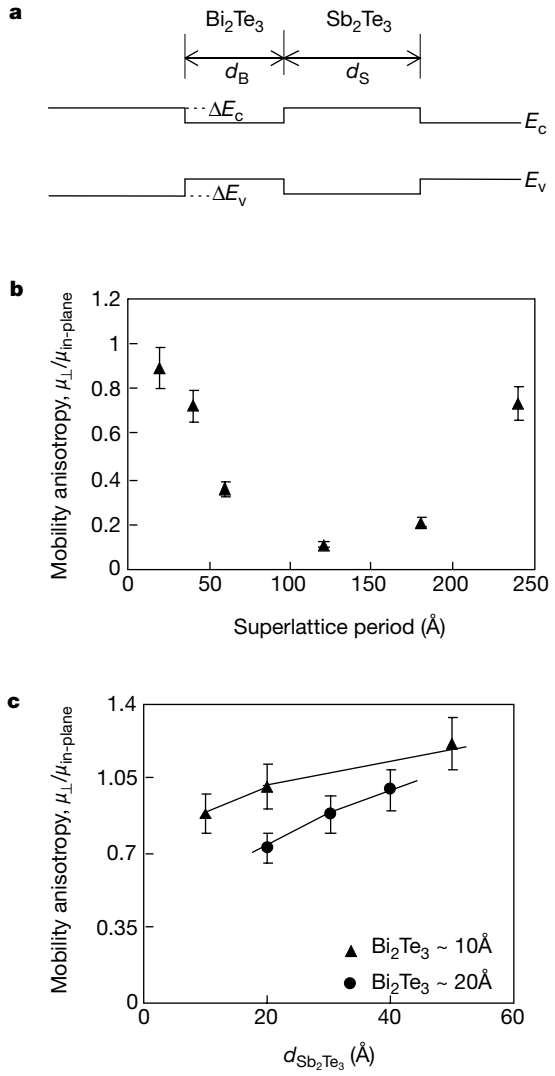

Figure 1 Hole transport across the Bi_2Te_3/Sb_2Te_3 superlattice interface. **a**, The anticipated heterojunction band diagram. $\Delta E_v + \Delta E_c < 2kT$, $\Delta E_v \approx kT$, $d_S + d_B =$ superlattice period (here ΔE_V and ΔE_c represent the valence and conduction band offsets, respectively, in the heterostructure, and $kT \approx 0.0285$ eV at 300 K. **b**, The observed hole mobility anisotropy versus superlattice period for the case of $d_B = d_S = (1/2)$ period. **c**, The hole mobility anisotropy in other Bi_2Te_3/Sb_2Te_3 superlattices.

© 2001 Macmillan Magazines Ltd

Table 1 Theoretical and experimental lattice thermal conductivities

Material	Thermal conductivity ($W m^{-1} K^{-1}$)
K_{min} of Bi_2Te_3 (*a-b* axis), Slack model[34]	0.55
K_{min} of Bi_2Te_3 (*c* axis), Slack model[34]	0.28
K_{min} of Bi_2Te_3 (*a-b* axis), Cahill model[35]	0.28
K_{min} of Bi_2Te_3 (*c* axis), Cahill model[35]	0.14
K_L of $Bi_{2-x}Sb_xTe_3$ alloy (*a-b* axis)	0.97
K_L of $Bi_{2-x}Sb_xTe_3$ alloy (*c* axis)	0.49
K_L of Bi_2Te_3/Sb_2Te_3 superlattice (*c* axis)	0.22

Lattice thermal conductivity (K_L) of the Bi_2Te_3/Sb_2Te_3 superlattice (period ~50 Å) compared with K_L observed in the respective alloys and the theoretical minimum lattice thermal conductivity (K_{min}) from various models.

Variable-thickness *ZT* measurements

ZT of a thermoelectric material can be obtained from a unipolar thermoelement across which a temperature difference is developed by the Peltier effect using a quasi-steady-state current[20]. The unipolar thermoelement consists of a mesa device with two ohmic contacts for current injection. One end of the device is effectively attached to a heat sink at a fixed temperature by being on a thermally conducting substrate. A schematic of the four-probe measurement is shown in Fig. 2a. A current (I) leads to ohmic (V_R) and Peltier (V_0) voltages across the thermoelement, with the total voltage V_T being $V_R + V_0$ at steady state. With current off, V_R decays within the dielectric relaxation time but V_0 decays according to the thermal time constant. V_R includes resistance from the bulk resistance of the mesa and from that of the two contacts (equation (3)).

$$V_R = \rho_\perp (l/a)I + 2(\rho_c/a)I \quad (3)$$

Here, $\rho_\perp$, ρ_c (in $\Omega\,cm^2$), l and a are respectively the cross-plane electrical resistivity of the superlattice, the average specific resistivity of the two contacts, and the height and the cross-sectional area of the device. V_0, given by equation (4) below, is affected by any difference in heating at the two contacts. As shown below, the ρ_c in the devices is rather small; hence, differences in the two contacts, causing any relative voltages, is even smaller. Even so, currents were reversed, and an average V_0 was used to account for minor differences.

$$V_0 = (\alpha_\perp^2/K_T)T(l/a)I \quad (4)$$

From equations (3) and (4), we get extrinsic or device figure of merit (ZT_e) as (V_0/V_R) shown in equation (5)[20] below. In thick (large-l) bulk elements, where $2(\rho_c/\rho_\perp l)$ is rather small, ZT_e approaches the intrinsic figure of merit (ZT_i) given by equation (1).

$$ZT_e = V_0/V_R = \{\alpha_\perp^2 T/K_T\rho_\perp\}[1 + 2(\rho_c/\rho_\perp l)]^{-1} \quad (5)$$

We can get $\rho_\perp$ and $(\alpha_\perp^2/K_T)T$, respectively, from the variation of V_R and V_0 with l (or mathematically equivalent, Il/a). Thus ZT_i is:

$$ZT_i = [\partial V_0/\partial(Il/a)]/[\partial V_R/\partial(Il/a)] \quad (6)$$

The data from variable-device-thickness experiments are shown in Fig. 2b and c. We point out that each data point in Fig. 2b and c is an average of 125 transient measurements, stored digitally and averaged out. The variable-thickness method for extracting ZT_i works for medium-to-good ρ_c, that is, medium-to-good device ZT_e shown in Fig. 2b and c, respectively. In Fig. 2b, we obtain ZT_e (given by V_0/V_R) for the largest mesa thickness of ~1.35 μm of ~0.66; even so, the ratio of the two slopes, from equation (6) above, gives a ZT_i of 2.07. The y-intercept of V_R versus Il/a is used to obtain ρ_c, $\sim 1.45\times10^{-7}\,\Omega\,cm^2$ for the sample in Fig. 2b. This is more than a factor of ten smaller than in bulk technology, but still high for thin-film devices, limiting the extrinsic ZT to ~0.66. In Fig. 2c, however, a combination of thicker 10Å/50Å Bi_2Te_3/Sb_2Te_3 superlattice (thickest mesa ~2.67 μm) and an improved ρ_c of

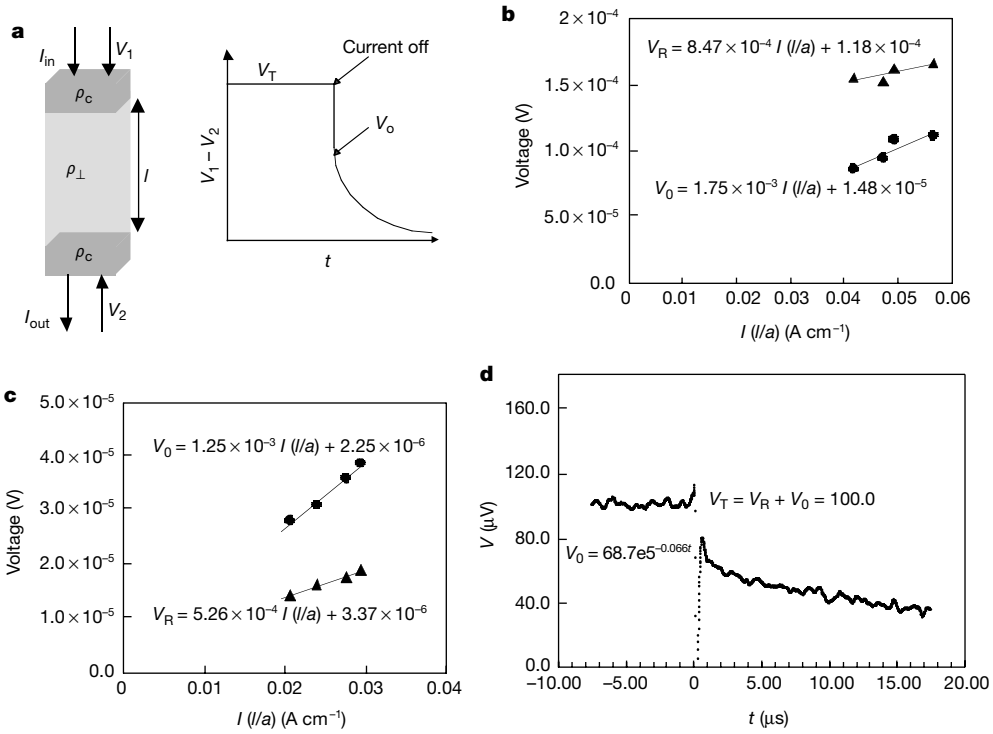

Figure 2 The *ZT* of a thermoelectric device. **a**, Direct measurement by a four-probe Harman method. (See text for definitions of symbols.) **b**, **c**, Variable-thickness *ZT* measurements. V_R and V_0 obtained from Harman method for each thickness indicate $ZT_i \approx 2.07$ and 2.34 in **b** and **c**, respectively. Working conditions: **b**, $I = 20.5$ mA and area, $4.9\times10^{-5}\,cm^2$; **c**, $I = 20.3$ mA and area, $1.8\times10^{-4}\,cm^2$. Triangles, V_R; circles, V_0. **d**, Harman-method transient on a 5.4-μm-thick 10Å/50Å Bi_2Te_3/Sb_2Te_3 superlattice device, shown for one current direction. The average extrinsic *ZT* for the two current directions is 2.38 ± 0.19. The voltage spike at $t \approx 0$, from momentary inductive coupling between the current and voltage circuits, prevents reliable determination of residual V_0 for $t < 1$ μs; thus extrapolation of data is used from $t > 1$ μs to get V_0. The transient is an average of 125 consecutive measurements, stored digitally and averaged out, which should lead to minimal error in extrapolation in spite of the spike.

© 2001 Macmillan Magazines Ltd

$1.5\times10^{-8}\,\Omega\,cm^2$ leads to a ZT_e value of ~2.04 for the thickest device. Based on the ratio of two slopes, a ZT_i of ~2.34 is deduced.

For the 10Å/50Å Bi_2Te_3/Sb_2Te_3 superlattice in Fig. 2b, the measured $\rho_\perp$ is $8.47\times10^{-4}\,\Omega\,cm$. With $\rho_{in\text{-}plane}$ of $9.48\times10^{-4}\,\Omega\,cm$, $\rho_\perp/\rho_{in\text{-}plane}$ or $\mu_\perp/\mu_{in\text{-}plane}$ is ~1.12. For the sample in Fig. 2c, $\rho_\perp$ is $5.26\times10^{-4}\,\Omega\,cm$ and $\rho_{in\text{-}plane}$ is $5.5\times10^{-4}\,\Omega\,cm$, thus giving an anisotropy of 1.05. These values are comparable to that indicated in Fig. 1c for the 10Å/50Å Bi_2Te_3/Sb_2Te_3 superlattice, confirming the ideal electron (hole) transmission characteristics of the structure.

Figure 2d shows the Harman-method transient[20] for a ~5.4-μm-thick 10Å/50Å Bi_2Te_3/Sb_2Te_3 superlattice thermoelement. The average ZT_e for two current directions was 2.38 ± 0.19 at 300 K. The material parameters for this superlattice film indicated a ZT_i of 2.59, and the measured ZT_e of 2.38 translates to a ρ_c of $\sim1.3\times10^{-8}\,\Omega\,cm^2$. Thus, going from a superlattice device of ~1.35 μm to ~2.67 μm to ~5.4 μm, we see no significant change in ZT_i and so the ZT_e begins to approach ZT_i because of a decreasing role of ρ_c.

As a check, we have measured ZT on 1-mm-thick and thinned-down (5–20 μm) thermoelements made from bulk p-type $Bi_xSb_{2-x}Te_{3-y}Se_y$ ($x\approx0.63\pm0.12$; $y\approx0.12$) alloys, comparable to those studied in ref. 3. The variable-thickness method indicates a ZT_i of ~1.09 at 300 K along the *a-b* axis in agreement with the results of ref. 3, indicating no unexpected benefits resulting from utilizing a thin-film version of the commercial material. Also, ZT in alloy films (non-superlattice structures) along the *c* axis were in the range of 0.4 ± 0.13 for carrier levels of $\sim3\times10^{19}\,cm^{-3}$, consistent with reported values for bulk materials[26].

Using temperature-dependent measurements of ρ, α and K_T of the p-type superlattice—and noting that there is little electrical anisotropy—the estimated ZT_i versus T of 10Å/50Å p-type Bi_2Te_3/Sb_2Te_3 superlattice is shown in Fig. 3, along with those of other materials. It appears that the superlattices would offer enhanced performance compared to the bulk p-type $Bi_{2-x}Sb_xTe_3$ alloys at lower temperatures. This is not surprising, given that the efficacy of superlattices in reducing K_L improves at lower temperatures as in Si/Ge superlattices[17]. As 'proof of advantage' of enhanced ZT at lower temperatures, we have obtained four times the cooling with Bi_2Te_3/Sb_2Te_3 superlattice devices compared to bulk p-type $Bi_{2-x}Sb_xTe_3$ devices at 210 K, for similar I/a, thermal load and parasitics. (Parasitics are unintentional heat losses from conductive, convective and any radiative processes.) Figure 3 shows that the p-type 10Å/50Å Bi_2Te_3/Sb_2Te_3 superlattice offers improved ZT compared to $CsBi_4Te_6$ alloy[11] at ~210 K.

Phonon-blocking/electron-transmitting structures

The results obtained with the 10Å/50Å Bi_2Te_3/Sb_2Te_3 superlattices indicate that we can fine-tune the phonon and hole (charge carriers) transport[37] to improve ZT. Other structures that show $ZT>1$ at 300 K include 10Å/40Å and 20Å/40Å Bi_2Te_3/Sb_2Te_3 superlattices. It is useful to compare the transport characteristics of phonons and holes. The product[38] kl_{mfp}, where k and l_{mfp} are respectively the average wavevector and mean free path, is used as a measure of the amount of blocking (or lack of it) for phonons and holes. For holes, we estimate the thermal velocity (v_{th}), de Broglie wavelength, and the wavevector magnitude as $\sim2.1\times10^7\,cm\,s^{-1}$, ~114 Å, and $\sim5.5\times10^6\,cm^{-1}$, respectively. From the relation[39] $(l_{mfp})_\perp\approx(v_{th}m^*\mu_\perp/q)$, we obtain $(l_{mfp})_\perp$ as 136 Å (for the sample with $ZT_i\approx2.34$, $\mu_\perp$ of $383\,cm^2\,V^{-1}\,s^{-1}$ is deduced from $\rho_\perp$, obtained from variable-thickness ZT). (Here m^* is the effective mass of charge carriers; holes in this case.) For an average phonon wavelength of ~30 Å and hole wavelength of ~114 Å, we obtain $(kl_{mfp})_{phonons}\approx0.5$ and $(kl_{mfp})_{holes}\approx7.6$. We believe that this comparison probably captures the phonon-blocking/electron-transmitting nature of certain superlattices[37].

n-type superlattices

We have also obtained encouraging results with n-type 10Å/50Å $Bi_2Te_3/Bi_2Te_{2.83}Se_{0.17}$ superlattices, indicating $ZT_i>1$ at 300 K. The variable-thickness ZT measurements, similar to those shown in Fig. 2b and c, indicate a ZT_i of ~1.46 at 300 K in these superlattices. The best extrinsic ZT_e for an n-type device has been ~1.2 at 300 K. The closeness of ZT_i and ZT_e is from obtaining a ρ_c value of $\sim1.2\times10^{-8}\,\Omega\,cm^2$. The cross-plane (along *c* axis) electrical resistivity in these n-type superlattices is $\sim1.23\times10^{-3}\,\Omega\,cm$, not significantly higher than the in-plane (along *a-b* axis) electrical resistivity of $1.04\times10^{-3}\,\Omega\,cm$. Thus in the 10Å/50Å n-type superlattices, apparently due to weak-confinement/near-zero band-offset, there is minimal anisotropy between in-plane and cross-plane electrical resistivities, similar to the 10Å/50Å and other p-type Bi_2Te_3/Sb_2Te_3 superlattices (Fig. 1c). The lack of electrical anisotropy in both the high-performance p-type and n-type superlattices, comparing properties along the *a-b* and *c* crystallographic axes, is in marked contrast to the electrical anisotropy observed in both p-type and n-type bulk materials[26].

The reason for the less-than-impressive ZT_i of 1.46 at 300 K in $Bi_2Te_3/Bi_2Te_{2.83}Se_{0.17}$ superlattices, compared to ~2.4 at 300 K in the best p-type Bi_2Te_3/Sb_2Te_3 superlattices, is its higher K_L. From its $\partial V_0/\partial(Il/a)$ and an α of $\sim238\,\mu V\,K^{-1}$, a cross-plane K_T of $\sim9.45\,mW\,cm^{-1}\,K^{-1}$ is obtained. Using the Weidemann–Franz law and a $\rho_\perp$ value of $1.23\times10^{-3}\,\Omega\,cm$, we obtain an electronic thermal conductivity of $\sim3.7\,mW\,cm^{-1}\,K^{-1}$. Thus the cross-plane lattice thermal conductivity is $\sim5.8\,mW\,cm^{-1}\,K^{-1}$. This is more like the *c*-axis K_L of bulk alloys[26]—and much higher than the value of $\sim2.5\,mW\,cm^{-1}\,K^{-1}$ observed in 60-Å-period p-type Bi_2Te_3/Sb_2Te_3 superlattices in ref. 29, and higher than that derived from the analysis of data in Figs. 2b, c. We believe that these results indicate near-ideal superlattice interfaces in the Bi_2Te_3/Sb_2Te_3 system[21], where the compositional modifications of either Bi or Sb are accomplished within regions enclosed by the Te–Te van der Waals bond. Thus, it should be possible to obtain mirror-like superlattice interfaces, leading to potential reflection effects for reducing K_L (ref. 29). In contrast, in the $Bi_2Te_3/Bi_2Te_xSe_{3-x}$ system, where both Se and Te are expected to be present at the van der Waals interface, we anticipate much unintended compositional mixing. Thus, the lattice thermal conductivity is likely to be more typical of an alloy. This was further evident in our observations of a lack of any significant improvement in electronic mobilities in n-type $Bi_2Te_3/Bi_2Te_{2.83}Se_{0.17}$ superlattices (compared to n-type $Bi_2Te_{3-x}Se_x$ alloys), in contrast to a marked enhancement of carrier mobilities observed in p-type Bi_2Te_3/Sb_2Te_3 superlattices relative to p-type $Bi_{2-x}Sb_xTe_3$ alloys[21]. Therefore, enhancement of ZT_i to 1.46 in n-type superlattices (from ~1 for bulk n-type alloy) appears to be attributable to the lack of electrical anisotropy and the typical lower lattice thermal conductivity associated with the *c* axis ($\sim5.8\,mW\,cm^{-1}\,K^{-1}$

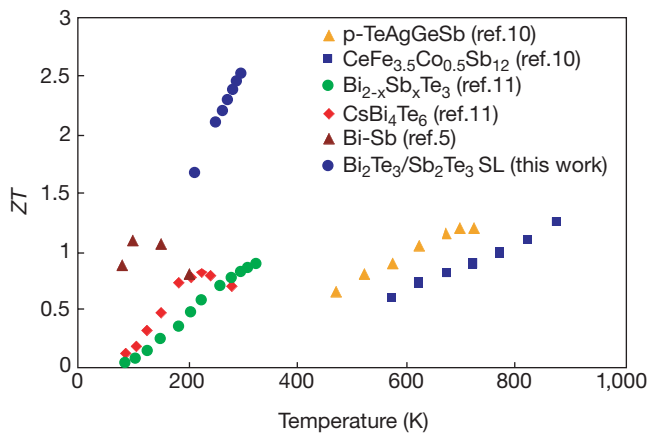

Figure 3 Temperature dependence of ZT of 10Å/50Å p-type Bi_2Te_3/Sb_2Te_3 superlattice compared to those of several recently reported materials.

© 2001 Macmillan Magazines Ltd

compared to ~10 mW cm^{-1} K^{-1} along the *a*-*b* axis). Better n-type superlattices with low K_L could be possible in those superlattices that have negligible compositional mixing at the van der Waals interface.

Thermoelectric devices for localized, rapid cooling/heating

Figure 4a shows the sub-ambient cooling obtained in a p-type superlattice device. With an ambient temperature $T_{ambient}$ of about 298 K, we have 32.2 K of cooling (down to −7 °C)—without any forced heat removal by blowing air or running water at the heat sink. Cooling was measured with 12.5-μm thermocouple wires (bead size ~50 μm). Thus the measured cooling is almost always with a load comparable to the thin-film device and in spite of the significant probe-heating on top of the mesa. Under similar testing conditions (same *l*/a, lack of heat removal at heat sink, residual thermal load/heat loss), we measured ~18.4 K of cooling in p-type bulk devices (Fig. 4a). In the linear regime (current < 1 A) where heat-sinking considerations are less, the superlattice device shows a factor of 2.2 cooling compared to bulk. We observed 40 K of cooling for the superlattice device when the heat sink is maintained at 353 K using a large-wattage heater, equivalent to a semi-infinite heat-source. This is analogous to the cooling of heat-sensitive devices in regions adjacent to hotspots in a chip. These results can be compared to recent measurements of cooling of 2.8 K and 6.9 K, measured using micro-thermocouples at 298 K and 373 K, respectively, in SiGeC/Si devices[40] of larger *l*/*a* ratio (~12.5).

Thin-film thermoelements lead to large cooling power densities (P_D) for similar maximum heat pumping (Q_m)[41] as per equation (7) below, following equation (1). As the area of the device, *a*, is reduced proportional to its thickness, *l*, Q_m is unaffected. However, cooling power density ($P_D \approx Q/a$) is increased. Here $T_{hot\text{-}side}$ and $T_{cold\text{-}side}$ refer to the absolute temperature of the hot and cold junctions, respectively, at either end of the active thermoelement.

$$Q_m = (a/l)\{[0.5\alpha^2 T^2_{cold-side}/\rho] - [K_T(T_{hot-side} - T_{cold-side})]\} \quad (7)$$

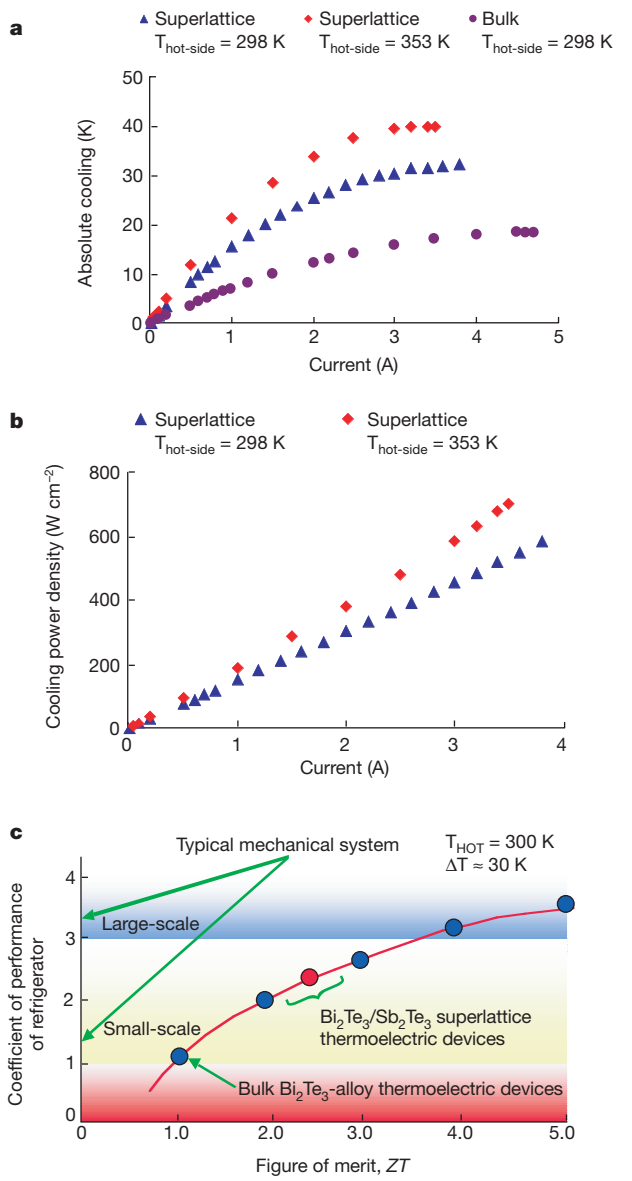

Figure 4 Cooling properties. **a**, Observed cooling as a function of current in a 150-μm circular device made from a p-type superlattice (data shown for hot side at 298 K (blue triangles) and 353 K (red diamonds)) is compared with that of a bulk device (hot side at 298 K, purple circles). **b**, Estimated cooling power density for superlattice devices as a function of current; blue triangles, hot side at 298 K, red diamonds, hot side at 353 K). **c**, Potential COP as a function of *ZT* with various technologies. T_{HOT} refers to the heat-sink temperature.

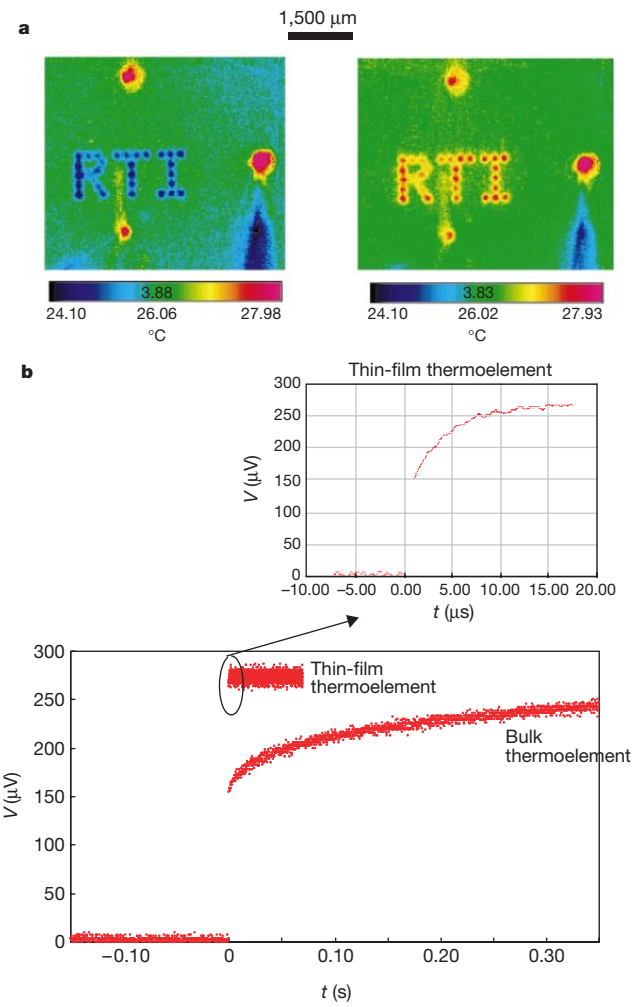

Figure 5 Demonstration of localized and high-speed cooling/heating obtainable with thin-film devices. **a**, Infrared images of spot cooling/heating with thin-film (p-type only) superlattice devices. Note current-injection areas (probes) do not change with current reversal; current through each element, ~65 mA. The infrared images of spots, corresponding to localized cooling or heating, spelling out RTI (Research Triangle Institute) were made using photolithographically processed micro-thermoelements. **b**, Comparison of thermal/cooling time response of thin-film (~5-μm) superlattice device and a bulk device.

© 2001 Macmillan Magazines Ltd

In addition to offering low ZT, which translates to low coefficient of performance (COP) in refrigeration, the bulk thermoelectric devices have low P_D ($\sim$1 W cm^{-2}), another disincentive for high-power electronic/microprocessor applications. Using the values of K_T and α of the superlattices, available P_D as a function of current is estimated in Fig. 4b for the superlattice device. We estimate a value of P_D of $\sim$700 W cm^{-2} at 353 K and $\sim$585 W cm^{-2} at 298 K at the measured maximum cooling in superlattice devices compared to a value of $\sim$1.9 W cm^{-2} in the bulk device of Fig. 4a. The effect of higher ZT on COP is shown in Fig. 4c. The translation of the device ZT to COP of refrigeration would involve efficient heat removal at the heat sink, reduction of thermal resistances at the interface between the active device and the two heat-spreaders, and the fabrication of p–n couples with minimal interconnect resistances. A sub-ambient cooling of 22.5 K at 300 K has been obtained in early p–n couples, currently limited by lower ZT of the n-thermoelement, large interconnect-resistance between the p- and n-thermoelements and absence of forced heat removal.

The thin-film devices also allow the concept of localized cooling by matching the footprint of the refrigeration devices to that of thermal load. This is made feasible by the combination of micro-electronic processing[42] and the ability to place the thermoelectric devices at points of interest; the reversal of current allows spot heating. This flexibility is demonstrated by the infrared images in Fig. 5a. In addition to placing cooling power where required, these thin-film superlattice thermoelements are fast-acting—about 23,000 times faster than bulk devices. This faster response is demonstrated in Fig. 5b. The thin-film device achieves steady-state cooling (indicated by the development of cooling-induced Seebeck voltage) in 15 μs, while the bulk thermoelement takes about 0.35 s. This is a result of the response time associated with the transport of heat through the thin film (micrometres) rather than through the millimetres associated with bulk devices. The thermal response time is about $4l^2/\pi^2 D$, where l is the thickness of the thermoelement and D is the thermal diffusivity. This rapid, high-performance cooling and heating, capable of high power densities and with the ability to be locally applied, could have applications in technologies ranging from genomic/proteomic chips to fibre-optic switching[37].

Power conversion with thin-film superlattice devices

We also tested the thin-film microdevices in a power-conversion mode. These superlattice thin-film devices, 5.2 μm thick, can develop a ΔT of 70 K across them, with a corresponding open-circuit voltage indicating an average α of $\sim$243 μV K^{-1}. The ΔT translates into a temperature gradient of $\sim$134,000 K cm^{-1}. The typical Seebeck coefficient suggests no unusual departure from classical behaviour at these gradients. Due to the higher ZT, modest power-conversion efficiencies can be achieved even for low ΔT. Lightweight, high-power-density devices could be useful for portable power and thermal scavenging.

Thin-film thermoelectric technology could be implemented in a modular fashion: that is, units of thin-film thermoelectric heat-pump or power-conversion devices could be scaled for various capacities. We have reported here several techniques that could be useful in creating such modules: the bonding of thin films to a heat sink, the removal of substrate, photo-lithography to achieve appropriate l/a ratios, the preparation of low-resistivity contacts, and the ability to preserve the properties of the nanometre-scale superlattices during detailed processing. □

Received 6 June; accepted 24 August 2001.

1. Ioffe, A. F. *Semiconductor Thermoelements and Thermoelectric Cooling* (Infosearch, London, 1957).
2. Wright, D. A. Thermoelectric properties of bismuth telluride and its alloys. *Nature* **181,** 834 (1958).
3. Ettenberg, M. H., Jesser, W. A. & Rosi, F. D. in *Proc. 15th Int. Conf. on Thermoelectrics* (ed. Caillat, T.) 52–56 (IEEE, Piscataway, NJ, 1996).
4. Polvani, D. A., Meng, J. F., Chandrashekar, N. V., Sharp. J. & Badding, J. V. Large improvement in thermoelectric properties in pressure-tuned p-type $Sb_{1.5}Bi_{0.5}Te_3$. *Chem. Mater.* **13,** 2068–2071 (2001).
5. Yim, W. M. & Amith, A. Bi-Sb alloys for magneto-thermoelectric and thermomagnetic cooling. *Solid State Electron.* **15,** 1141–1165 (1972).
6. Vining, C. B. in *Proc. 11th Int. Conf. on Thermoelectrics* (ed. Rao, K. R.) 276–284 (Univ. Texas at Arlington, 1992).
7. Slack, G. A. & Tsoukala, V. G. Some properties of semiconducting $IrSb_3$. *J. Appl. Phys.* **76,** 1665–1671 (1994).
8. Sales, B. C., Mandrus, D. & Williams, R. K. Filled skutterudite antimonides: a new class of thermoelectric materials. *Science* **272,** 1325–1328 (1996).
9. Mandrus, D. *et al.* Filled skutterudite antimonides: Validation of the electron-crystal phonon-glass approach to new thermoelectric materials. *Mater. Res. Soc. Symp. Proc.* **478,** 199–209 (1997).
10. Fleurial, J. P. *et al.* in *Proc. 15th Int. Conf. on Thermoelectrics* (ed. Caillat, T.) 91–95 (IEEE, Piscataway, NJ, 1996).
11. Chung, D. Y. *et al.* $CsBi_4Te_6$: A high-performance thermoelectric material for low-temperature application. *Science* **287,** 1024–1027 (2000).
12. Tritt, T. M., Kanatzidis, M. G., Lyon, H. B. Jr & Mahan, G. D. Thermoelectric materials—New directions and approaches. *Mater. Res. Soc. Proc.* **478,** 73–84 (1997).
13. Hicks, L. D. & Dresselhaus, M. D. Effect of quantum-well structures on the thermoelectric figure of merit. *Phys. Rev. B* **47,** 12727–12731 (1993).
14. Harman, T. C., Taylor, P. J., Spears, D. L. & Walsh, M. P. in *Proc. 18th Int. Conf. on Thermoelectrics* (ed. Ehrlich, A.) 280–284 (IEEE, Piscataway, NJ, 1999).
15. Venkatasubramanian, R. *et al.* in *Proc. 1st Natl Thermogenic Cooler Workshop* (ed. Horn, S. B.) 196–231 (Center for Night Vision and Electro-Optics, Fort Belvoir, VA, 1992).
16. Venkatasubramanian, R. Thin-film superlattice and quantum-well structures—a new approach to high-performance thermoelectric materials. *Naval Res. Rev.* **58,** 31–40 (1996).
17. Lee, S. M., Cahill, D. G. & Venkatasubramanian, R. Thermal conductivity of Si-Ge superlattices. *Appl. Phys. Lett.* **70,** 2957–2959 (1997).
18. Mahan, G. D. & Woods, L. M. Multilayer thermionic refrigeration. *Phys. Rev. Lett.* **80,** 4016–4019 (1998).
19. Shakouri, A. & Bowers, J. E. Heterostructure integrated thermionic coolers. *Appl. Phys. Lett.* **71,** 1234–1236 (1997).
20. Harman, T. C., Cahn, J. H. & Logan, M. J. Measurement of thermal conductivity by utilization of the Peltier effect. *J. Appl. Phys.* **30,** 1351–1359 (1959).
21. Venkatasubramanian, R. *et al.* Low-temperature organometallic epitaxy and its application to superlattice structures in thermoelectrics. *Appl. Phys. Lett.* **75,** 1104–1106 (1999).
22. Venkatasubramanian, R. Low temperature chemical vapor deposition and etching apparatus and method. US Patent No. 6071351 (6 June 2000).
23. Venkatasubramanian, R. in *Recent Trends in Thermoelectric Materials Research III* (ed. Tritt, T. M.) Ch. 4 (Academic, San Diego, 2001).
24. Berger, H. H. Models for contacts to planar devices. *Solid State Electron.* **15,** 145–158 (1972).
25. Drabble, J. R., Groves, R. D. & Wolfe, R. Galvanomagnetic effects in n-type Bi_2Te_3. *Proc. Phys. Soc.* **71,** 430–434 (1957).
26. Scherrer, H. & Scherrer, S. in *CRC Handbook of Thermoelectrics* (ed. Rowe, D. M.) 211–237 (CRC Press, Boca Raton, FL, 1995).
27. Palmier, J. F. in *Heterojunctions and Semiconductor Superlattices* (eds Allan, G., Bastard, G., Boccara, N., Launoo, N. & Voos, M.) 127–145 (Springer, Berlin,1986).
28. Cappaso, F., Mohammed, K. & Cho, A. Y. Resonant tunneling through double barriers, perpendicular quantum transport phenomena in superlattices, and their device applications. *IEEE J. Quant. Electron.* **QE-22,** 1853–1869 (1986).
29. Venkatasubramanian, R. Lattice thermal conductivity reduction and phonon localizationlike behavior in superlattice structures. *Phys. Rev. B* **61,** 3091–3097 (2000).
30. Narayanamurti, V., Störmer, H. L., Chin, M. A., Gossard, A. C. & Weigmann, W. Selective transmission of high-frequency phonons by a superlattice: the dielectric phonon filter. *Phys. Rev. Lett.* **43,** 2012–2015 (1979).
31. John, S. Strong localization of photons in certain disordered dielectric superlattices. *Phys. Rev. Lett.* **58,** 2486–2489 (1987).
32. Wiersma, D. S., Bartolini, P., Lagendik, A. & Righini, R. Localization of light in a disordered medium. *Nature* **390,** 671–673 (1997).
33. Simkin, M. V. & Mahan, G. D. Minimum thermal conductivity of superlattices. *Phys. Rev. Lett.* **84,** 927–930 (2000).
34. Slack, G. in *Solid State Physics*, 1–71 (eds Ehrenreich, H., Seitz, F. & Turnbull, D.) Series 34 (Academic, New York, 1979).
35. Cahill, D. G., Watson, S. K. & Pohl, R. O. Lower limit to the thermal conductivity of disordered crystals. *Phys. Rev. B* **46,** 6131–6140 (1992).
36. Goldsmid, H. J. in *Proc. 18th Int. Conf. on Thermoelectrics* (ed. Ehrlich, A.) 531–535 (IEEE Press, Piscataway, NJ, 1999).
37. Venkatasubramanian, R. *Thin-film Thermoelectric Cooling and Heating Devices for DNA Genomics/ Proteomics, Thermo-Optical Switching-Circuits, and IR Tags* (US Patent Filing, Ser. No. 60/282,185, 2001).
38. Sheng, P. *Introduction to Wave Scattering, Localization, and Mesoscopic Phenomena* (Academic, London, 1995).
39. Kittel, C. *Introduction to Solid State Physics* (Wiley, New York, 1976).
40. Fan, X. *et al.* SiGeC/Si superlattice microcoolers. *Appl. Phys. Lett.* **78,** 1580–1582 (2001).
41. Cadoff, I. B. & Miller, E. *Thermoelectric Materials and Devices* (Reinhold, New York, 1960).
42. Venkatasubramanian, R. Thin-film thermoelectric device and fabrication method of same. US Patent No. 6300150 (9 October 2001).

Acknowledgements

This work was supported by the US Defense Advanced Research Projects Agency and the US Office of Naval Research.

Correspondence and requests for materials should be addressed to R.V. (e-mail: rama@rti.org).

© 2001 Macmillan Magazines Ltd